**ciRS-7 exonic sequence is embedded in a long non-coding RNA locus**

Steven P. Barrett[1¶], Kevin R. Parker[2¶], Caroline Horn[1], Miguel Mata[3], Julia Salzman[1,4*]

[1]Department of Biochemistry, Stanford University School of Medicine, Stanford, CA, USA

[2]Institute for Stem Cell Biology and Regenerative Medicine, Stanford University School of Medicine, Stanford, CA, USA

[3] Department of Microbiology and Immunology, Stanford University School of Medicine, Stanford, CA, USA

[4] Department of Biomedical Data Science, Stanford University School of Medicine, Stanford, CA, USA

*correspondence to:
julia.salzman@stanford.edu

[¶]These authors contributed equally to this work.

## Abstract

ciRS-7 is an intensely studied, highly expressed and conserved circRNA. Essentially nothing is known about its biogenesis, including the location of its promoter. A prevailing assumption has been that ciRS-7 is an exceptional circRNA because it is transcribed from a locus lacking any mature linear RNA transcripts of the same sense. Our interest in the biogenesis of ciRS-7 led us to develop an algorithm to define its promoter. This approach predicted that the human ciRS-7 promoter coincides with that of the long non-coding RNA, LINC00632. We validated this prediction using multiple orthogonal experimental assays. We also used computational approaches and experimental validation to establish that ciRS-7 exonic sequence is embedded in linear transcripts that are flanked by cryptic exons in both human and mouse. Together, this experimental and computational evidence generate a new view of regulation in this locus: (a) ciRS-7 is like other circRNAs, as it is spliced into linear transcripts; (b) expression of ciRS-7 is primarily determined by the chromatin state of LINC00632 promoters; (c) transcription and splicing factors sufficient for ciRS-7 biogenesis are expressed in cells that lack detectable ciRS-7 expression. These findings have significant implications for the study of the regulation and function of ciRS-7, and the analytic framework we developed to jointly analyze RNA-seq and ChIP-seq data reveal the potential for genome-wide discovery of important biological regulation missed in current reference annotations.

## Author Summary

circRNAs were recently discovered to be a significant product of ‘host’ gene expression programs but little is known about their transcriptional regulation. Here, we have studied the expression of a well-known circRNA named ciRS-7. ciRS-7 has an unusual function for a circRNA; it is believed to be a miRNA sponge. Previously, ciRS-7 was thought to be transcribed

from a locus lacking any mature linear isoforms, unlike all other circular RNAs known to be expressed in human cells. However, we have found this to be false; using a combination of bioinformatic and experimental genetic approaches, in both human and mouse, we discovered that linear transcripts containing the ciRS-7 exonic sequence, linking it to upstream genes. This suggests the potential for additional functional roles of this important locus and provides critical information to begin study on the biogenesis of ciRS-7.

## Introduction

Until recently, the expression of circRNA was almost completely uncharacterized, with a few important exceptions [1–4]. It is now appreciated that circRNAs are a ubiquitous feature of eukaryotic gene expression [1,3,5,6]. While many functions have been posited for circRNAs, few have been supported with experimental evidence. ciRS-7, one of the most highly expressed and most intensely studied circRNAs, is an exception to this rule, where recent work has shown it functions as a miRNA sponge [6,7]. The sequence of ciRS-7 is highly repetitive with over 70 repeated miR-7 seed sequences in humans, most of which are conserved across eutherian mammals, and its expression is highly variable across tissues [6–8]. ciRS-7 also exhibits increasing expression in neuronal differentiation models *in vitro [9]*. In zebrafish, which do not have an endogenous copy of ciRS-7 but do express miR-7, ectopic expression of the ciRS-7 sequence results in a defect in midbrain development [6]. And a recent ciRS-7 knock-out mouse exhibited neuronal defects, including impaired sensorimotor gating and dysfunctional synaptic transmission [10]. In spite of these functional findings, a model for the biogenesis and regulation of ciRS-7 is lacking, and key questions remain: What is the primary transcript that is processed to produce ciRS-7? Where in the genome is the promoter for this transcript? Are there any other spliced transcripts, circular or linear, generated from this locus?

71 Correlative and mini-gene analyses have suggested that biogenesis of some circRNAs
72 is regulated by intronic sequence flanking the circularized exon [11–13]. However, the
73 immediate flanking sequence does not appear to control the biogenesis of ciRS-7; inserting 1 kb
74 of the endogenous sequence flanking the ciRS-7 exon into a plasmid driven by a CMV promoter
75 was not sufficient to produce ciRS-7 [7], implying that additional sequence is necessary for
76 circularization. Identifying this additional sequence is an especially difficult problem in the case
77 of ciRS-7, as the intron upstream of the circularized exon has not been described due to the
78 lack of an annotated promoter, and unlike every other known human circular RNA, ciRS-7 is not
79 thought to be included in a mature linear transcript, obscuring possible transcriptional start sites
80 that would be shared with these isoforms.

81 Identifying the promoter for ciRS-7 has broad implications but is non-trivial: unlike for
82 linear RNAs where techniques like 5' RACE can determine the transcription start site (TSS), no
83 such approach can be used for ciRS-7 or any other circRNA. To overcome this problem and to
84 identify the TSS of ciRS-7 , we designed a new statistical method that entailed integrative
85 analysis of chromatin modifications measure by ChIP and the RNA expression levels of ciRS-7
86 to identifying its promoter. This is a general analytic framework that could be applied to any
87 transcript, but we chose to focus on ciRS-7 because of the biological significance described
88 above and because it has stood out as the only case of a human circRNA with no known linear
89 counterpart.

90 Our analysis led us to discover that the promoters of a nearby uncharacterized locus
91 currently annotated as a long non-coding RNA (LINC00632) were responsible for driving ciRS-7
92 expression. In contrast to current thinking in the field, we also discovered that, in both human
93 and mouse, the ciRS-7 exon is embedded in novel linear transcripts that include cryptic exons
94 both up and downstream of the ciRS-7 sequence. In humans, these linear transcripts include
95 exons overlapping with LINC00632, and the subcellular localization of transcripts from
96 LINC00632 vary depending on the presence of the ciRS-7 sequence.

Together, these results support (post-)transcriptional coupling between a long-noncoding RNA and ciRS-7 and raise important functional questions about this locus. Our results also represent the first steps toward pinpointing the mechanisms underlying the regulation and biogenesis of ciRS-7.

## Results

### Computational methods predict the ciRS-7 promoter region

As a first step to identify the ciRS-7 promoter, we examined available chromatin immunoprecipitation sequencing (ChIP-seq) data from HeLa, HEK293, and *in vitro* differentiated neuronal cells, which exhibit a range of ciRS-7 expression, from very low (or nonexistent) in HeLa cells to very high in neurons [7–9].

We investigated RNA Polymerase II binding as well as the histone modifications H3K4me3 and H3K27ac, which are enriched in active promoters [14,15]. In addition, we examined H3K4me1, which is enriched in enhancers, and H3K27me3, a repressive mark enriched in silenced loci [16]. The only peaks called by MACS2, a widely used peak-calling algorithm [17], in H3K4me3, H3K27ac or RNA Polymerase II were in HEK293 and *in vitro* differentiated neuronal cells and coincided with the transcriptional start positions of LINC00632 isoforms, the nearest annotated transcript upstream of ciRS-7 (Fig 1A; S1 Fig). Conversely, the repressive mark H3K27me3 was visibly enriched throughout the LINC00632 and ciRS-7 locus in HeLa cells, consistent with their lack of ciRS-7 expression, with a H3K27me3 peak called at a LINC00632 promoter (S1 Fig). This visual inspection generated the hypothesis that the LINC00632 and ciRS-7 promoters coincide, which we went on to quantitatively test.

If ciRS-7 shares its promoter with LINC00632, activating chromatin marks at the LINC00632 promoter and ciRS-7 expression should be positively correlated. To test this prediction, we analyzed matched ChIP-seq and RNA-seq data from 34 ENCODE tissues and

122 cell types. Specifically, we separated the ~175 kb genomic region spanning 50 kb upstream of
123 the LINC00632 annotation to 50 kb downstream of ciRS-7into 500 bp bins, and we computed
124 the Pearson correlation between ciRS-7 expression and the enrichment of each of three
125 activating marks (H3K4me3, H3K4me1, and H3K27ac) in each bin (Fig 1B). Because the null
126 distribution of the Pearson correlation requires assumptions that do not hold for our data, we
127 computed an empirical null distribution: for each activating mark, we computed the Pearson
128 correlation between ciRS-7 expression and its enrichment per bin 50 kb up- and downstream of
129 genes that should have no relationship to expression or chromatin modifications in the ciRS-7
130 locus: ACTB, HOTAIR, and FOXO4. This empirical null distribution was used to estimate the
131 FDR for the correlation coefficients at each bin/mark pair (S2 Fig, Methods).
132 The Pearson correlation between H3K4me3 marks and ciRS-7 expression were highest
133 and statistically significant ($q<0.005$) at the two promoters of LINC00632 (Fig 1C, marked as
134 'P(Distal)' and 'P(Proximal)'; S3 Fig) and H3K27ac marks in these regions were also high and
135 statistically significant ($q<0.005$). Coincident H3K4me1 and H3K27ac marks, marks of active
136 enhancers [18], found in this loci were also significantly correlated with ciRS-7 expression (Fig
137 1C, marked as 'E'). No significant signal at regions more proximal to the ciRS-7 exon or
138 upstream of annotated LINC00632 isoforms were observed, providing further statistical support
139 that ciRS-7 expression is driven from these promoters.
140
141 **Orthogonal experimental tests validate that ciRS-7 shares a promoter with LINC00632**
142 To determine whether specific activation of the LINC00632 promoters was sufficient to drive
143 ciRS-7 expression, we used three experimental tests. First, we used the promoter-activating
144 CRISPRa system in HeLa cells which express low or undetectable levels of ciRS-7[7,19] to test
145 if ciRS-7 expression could be driven by these promoters. We designed single guide RNAs
146 (sgRNAs) to target the two promoter regions highlighted in Fig 1C, just upstream of T1 and T3,
147 identified as the putative promoter regions by computational analysis (See S1 File for sgRNA

148 sequences). Targeting of the CRISPRa system to either region resulted in induction of specific
149 LINC00632 isoforms, and activating either of these promoters induced robust expression of
150 ciRS-7 (Fig 2A), with a ∆Ct compared to ACTB of ~10 (S4 Fig), although at ~2-3 orders of
151 magnitude less than in the highly expressing HEK293 cells.

152 To test the hypothesis that HeLa cells are competent to express ciRS-7 at the nearest
153 identified promoter if it is free from repressive chromatin marks, we transfected a Bacterial
154 Artificial Chromosome (BAC O, Fig 2B), containing a genomic fragment starting upstream of the
155 proximal LINC00632 promoter and ending ~50 kb downstream of ciRS-7, into HeLa cells. We
156 detected significant expression of ciRS-7 and LINC00632 from this BAC by both RT-PCR and
157 Northern blot after one day of transfection. As an aside, this experiment supports the model that
158 the lack of LINC00632 and ciRS-7 expression in HeLa cells is due to chromatin modification of
159 the locus, rather than the absence of necessary trans-acting factors and shows that all (post-
160 )transcriptional machinery required for ciRS-7 expression are present in HeLa cells (Fig 2C,D;
161 S5 Fig).

162 As an orthogonal test that the proximal LINC00632 promoter, and no further downstream
163 promoter drives ciRS-7 expression, we transfected three other BACs (A-C) each containing the
164 exonic sequence of ciRS-7, but differing in their inclusion of the proximal endogenous promoter
165 of LINC00632 (Fig 2B,E). Because BAC O transfects more efficiently than BACs A-C, likely due
166 to its relatively small size, we excluded it in this comparison (S6 Fig). Expression of LINC00632
167 isoforms and ciRS-7 were correlated and highly dependent on inclusion of the LINC00632
168 promoter, further supporting the hypothesis that ciRS-7 and LINC00632 isoforms share the
169 same promoters (Fig 2E, S7A Fig).

170 As a final test that the dominant promoter of ciRS-7 is located in the LINC00632
171 promoter, we created a genomic deletion in HEK293T cells, which express ciRS-7 at high levels
172 [8], that encompasses the predicted positions of both putative promoters and encompass the

173 guide RNAs used for CRISPRa (hg38 coordinates, chrX:140,709,590-140,749,836) (see
174 diagram in S7B Fig). We obtained one homozygous clone. ciRS-7 decreased by approximately
175 one thousand-fold (S7B Fig), but was not completely abolished, reflecting residual low-level
176 promoter activity in the LINC00632 locus.
177
178 **ciRS-7 is an exon embedded in mature human and mouse linear RNA transcripts**
179 In parallel with our computational approach to identify the promoter of ciRS-7, we tested
180 whether gaps in the reference annotation of human exons might have missed upstream and or
181 downstream exons spliced to and/or from ciRS-7. Indeed, spliceosomal circRNAs contain both
182 5' and 3' splice sites flanking their exons, and in almost all known cases, circRNA exons are
183 embedded in linear transcripts spliced to and from downstream and upstream exons [1,3].
184 We developed an analysis of RNA-seq reads capable of detecting splicing outside of
185 annotated exonic sequences, as most algorithms that do not use annotations have high false
186 positive and negative rates [20]. We took a transparent, simple two-step approach in an effort to
187 establish existence of exons spliced to and from ciRS-7: In step 1, all reads are aligned to the
188 full genome and transcriptome; in step 2, unaligned reads are broken into two pseudo paired-
189 end reads and aligned to a 100 kb radius of ciRS-7 on chromosome X (Fig 3, upper; see
190 Methods for details). Rather than attempting to pinpoint a genomic breakpoint, this algorithm
191 reports all reads whose pseudo-paired ends map to the reference genome (File S2). Differences
192 in alignment positions of the two pseudo paired-end reads are used to infer the existence of
193 splicing events. As a positive control for this algorithm, we omitted the ciRS-7 junction from our
194 transcriptome index and attempted to (re-)discover this junction *de novo* and other un-annotated
195 splicing events.
196 We applied this algorithm to an H1 hESC RNA-seq dataset (Methods). 58 total reads
197 representing possible novel junctions near the ciRS-7 locus were identified, 55 of which could
198 be explained by the ciRS-7 circle junction. Of the three remaining reads, one represented a

199 novel junction between a cryptic donor site in the final exon of LINC00632 and the ciRS-7
200 acceptor and a second predicted splicing between the 3' end of ciRS-7 to a cryptic downstream
201 exon lacking any annotation (Fig 3, lower); a final read mapped internally to ciRS-7.
202 To test these novel predicted splicing events, we performed RT-PCR using primers in
203 HEK293T (Fig 4A,B; S8 Fig), a cell line known to express ciRS-7 [8]. Direct Sanger sequencing
204 of resulting products validated our predictions, and included two cryptic 5' splice sites in the final
205 exon of LINC00632 paired with the annotated acceptor of ciRS-7 (S9 Fig). RT-PCR for the
206 downstream exon yielded two splice isoforms, one of which was predicted computationally and
207 the other using an acceptor ~1 kb upstream (Fig 4C, S9 Fig, S10 Fig). qPCR for three variants:
208 LINC00632, the LINC00632-ciRS-7 transcript, and ciRS-7 in HEK293T showed that ciRS-7 was
209 ~250-fold more abundant than the LINC00632-ciRS-7 transcript and about ~50-fold more
210 abundant than LINC00632 (S11 Fig). LINC00632-ciRS-7 and LINC00632 transcripts were also
211 RNase R sensitive, as expected for linear transcripts (S12 Fig).
212 In an effort to test transcriptional co-regulation between LINC00632 and LINC00632-
213 ciRS-7, we profiled 136 ENCODE cell lines and tissues to quantify both (a) the total expression
214 of ciRS-7 sequence compared to LINC00632 and (b) the splice variants ciRS-7 and ciRS-7-
215 LINC00632 (S13 fig). This analysis revealed that (a) ciRS-7 is more highly expressed in
216 muscle and fat tissues than in the brain (based on TPM values); (b) the expression of
217 LINC00632-ciRS-7 splicing versus ciRS-7 expression is tissue-specifically regulated; and (c)
218 while relative expression levels of LINC00632 and ciRS-7 have a dynamic range across several
219 orders of magnitude, their expression was highly correlated across all cell lines and tissues we
220 analyzed (Pearson r=0.57, Spearman r=0.41, both p-vals<<10e-6). Together, this analysis
221 suggests both transcriptional coupling and differential regulation of splicing between LINC00632
222 and ciRS-7.
223 Many features of ciRS-7 expression are conserved in mammals [6]. We hypothesized
224 that its embedding in linear transcripts was similarly conserved, despite the current thinking that

225 ciRS-7 lacks a mature linear transcript in mammals [6–8,10,21]. To test this hypothesis, we
226 applied the the same analytic approach used above in human cells to mouse (Methods). It also
227 predicted the existence of novel cryptic exons flanking ciRS-7, variants that were confirmed by
228 RT-PCR in mouse brain (Fig 4D,E). In addition, it predicted a new circRNA resulting from back-
229 splicing of a cryptic exon 15 kb downstream of ciRS-7 to its annotated acceptor, which we
230 validated by PCR and sequencing (Fig 4D,E). qPCR for the linear junction between the novel
231 upstream exon and ciRS-7 showed this isoform was RNase R sensitive, evidence of it being
232 linear, and ~250 fold less abundant than ciRS-7 (S14 Fig). In this experiment, ciRS-7 was also
233 strongly sensitive to RNase R, as has been reported by others [3]. While exonic sequences
234 flanking ciRS-7 in linear transcripts have no detectable primary sequence homology between
235 human and mouse, such conservation is not necessarily expected for long non-coding RNAs
236 [22].
237 Our RNA-seq analysis focused on establishing the existence of cryptic exons spliced to
238 and from the ciRS-7 exon, rather than complete annotation of all existing transcripts. We sought
239 to estimate transcript diversity in this locus by exploratory RT-PCR in human cells. This work
240 uncovered isoforms that splice directly from LINC00632 to cryptic exons downstream of ciRS-7,
241 including skipping of the ciRS-7 sequence and direct splicing into the downstream internal exon
242 of ciRS-7 (Fig 4E, S10 Fig). We attempted several PCRs not guided by the RNA-seq analysis
243 described above; in general, these PCR reactions were negative, evidence against a model of
244 pervasive noisy splicing in the locus, and evidence that we had identified the dominant
245 transcripts expressed from the LINC00632 locus.
246
247 **ciRS-7 sequence has potential circRNA-independent regulatory effects**
248 To test for potential differential regulation of ciRS-7, LINC00632, and LINC00632-ciRS-7
249 linear transcripts, we profiled their subcellular localization by fractionating nuclear and
250 cytoplasmic RNA from HEK293T. Using XIST and ACTB as controls for enrichment of nuclear

251 and cytoplasmic fractions, respectively, qPCR demonstrated that, relative to ciRS-7, LINC00632
252 and LINC00632-ciRS-7 were enriched in the nucleus with increasing degrees (~9 and 25-fold
253 respectively vs. ciRS-7), suggesting that the ciRS-7 sequence impacts the steady-state
254 localization of transcripts containing it (Fig 4F).

255 One hypothesis generated by this work is that the expression of ciRS-7 is directly or
256 indirectly tied to the expression of other transcripts in this locus. The recent study that knocked
257 out the ciRS-7 sequence in mouse allows us to begin to test this hypothesis [10].

258 While we have not experimentally validated the transcriptional start of the ciRS-7 pre-
259 mRNA in mouse, there are many similarities to the human locus: the nearest upstream gene is
260 an uncharacterized lincRNA (C230004F18Rik) and the nearest H3K4me3 (a mark of promoter
261 activity) and RNA Polymerase II peaks to ciRS-7 occur at the transcriptional start of this lincRNA
262 (Fig 5A). In addition, transcription of this locus appears to begin at the C230004F18Rik
263 promoter, proceeding continuously past the ciRS-7 locus (Fig 5A). Taken together, these data
264 suggest that the transcriptional start of the ciRS-7 pre-mRNA in mouse occurs at an upstream
265 lincRNA, namely C230004F18Rik, as it does in human. This raises the question: is the
266 abundance of C230004F18Rik affected by the presence or absence of the ciRS-7 sequence?

267 To test this, we re-analyzed data from mouse ciRS-7 knockout experiment to determine
268 if deletion of the ciRS-7 sequence resulted in differential expression of C230004F18Rik. We
269 discovered that, when collapsing across all brain regions profiled, among differentially
270 expressed genes that are statistically significant, C230004F18Rik is the third-most upregulated
271 gene in the ciRS-7 KO vs. WT (Fig 5B,C; 2.44 fold induction, p-adjusted 1.21e-6). The most
272 upregulated gene is Fos (3.44 fold, p-adjusted 2.95e-5), and the second-most upregulated gene,
273 C030023E24Rik (3.03 fold, p-adjusted 1.10e-9), is an uncharacterized transcript located roughly 5.5
274 kb downstream of ciRS-7 and encompassed by the transcriptional read-buildup (Fig 5A-C).

275 In the hippocampus, C230004F18Rik was the most significantly changed gene after
276 ciRS-7 by p-value, with 3.11 fold higher expression (p-adjusted 2.51e-13), followed by

277 C030023E24Rik (3.4 fold higher, p-adjusted 6.29e-13) (S15 Fig). And C230004F18Rik was
278 significantly upregulated in all tissues examined except the cortex (S15 Fig) (the lack of
279 significant differential expression was presumably due to higher variability between replicates
280 than in other tissues, see Fig 5C). This consistent and large effect of ciRS-7 knock-out on
281 C230004F18Rik is consistent with a direct regulatory impact of the ciRS-7 sequence on
282 C230004F18Rik abundance.
283

284 ## Discussion

285 The embedding of ciRS-7 sequence in cryptic exons changes the view of the
286 exceptionality of ciRS-7 as circRNA lacking a linear host transcript: its transcriptional regulation
287 is similar to other circRNAs that are embedded in linear 'host' RNAs. In human, we have
288 computationally and experimentally demonstrated that LINC00632 and ciRS-7 share the same
289 promoters, and have strong support for a similar model in mouse from: (a) RNA-seq analysis
290 showing strong expression effects on flanking linear Riken transcripts from ciRS-7 KO; (b) RNA-
291 seq and PCR data linking ciRS-7 to cryptic up- and downstream exons; and (c) continuous
292 RNA-seq signal across the locus starting from the upstream gene C230004F18Rik, through
293 ciRS-7, and into the downstream transcript C030023E24Rik. Together, these data support the
294 model that C230004F18Rik, ciRS-7 and C030023E24Rik represent a single transcriptional
295 locus.
296 Because of the syntenic hosting of ciRS-7 in linear transcripts, and to simplify
297 nomenclature, we propose renaming the uncharacterized gene LINC00632 (respectively Riken
298 transcripts) to **A**lternatively **S**pliced **IN**to **C**iRS-7 (ASINC, respectively Asinc in mouse); we call
299 the linear variants of these non-coding RNAs lacking ciRS-7 sequence ASINC.1 and those
300 containing it ASINC.2.

301 The transcriptional and splicing machinery necessary for ciRS-7 expression is likely not
302 brain specific, and rather is general: BACs containing a fragment of the LINC00632 locus that
303 includes its promoter can express ciRS-7 when introduced to HeLa cells (which have little to no
304 endogenous expression of ciRS-7). ciRS-7 expression may be primarily regulated at the level of
305 chromatin modification of the locus, either at the newly-discovered promoters or putative
306 enhancers.

307 Our work has implications for the assigned functions of ciRS-7. Despite intensive study,
308 the promoter and mechanisms regulating ciRS-7 expression have remained mysterious. To
309 date, experiments studying the function of the ciRS-7 sequence have made what was a
310 reasonable simplifying assumption that the only transcripts containing the ciRS-7 sequence are
311 circular [8,10]. However, interpretation of past and future studies assigning function to the ciRS-
312 7 sequence must be made in light of its origination from and potential functions in linear
313 transcripts. This includes a recent study of a mouse model where the ciRS-7 exon was deleted
314 [10]. Our analysis of the ciRS-7 locus shows that knock-out of this exon results in an
315 upregulation of both the upstream and downstream Riken transcripts, C230004F18Rik and
316 C030023E24Rik. The magnitude and significance of these effects compared to other gene
317 expression changes suggests it was a direct effect of the ciRS-7 knockout, and raises the
318 possibility that some functions assigned to the knock-out animal could be due to increases in
319 expression of the Riken transcripts.

320 There are multiple models that could explain the increased expression of the up-and
321 downstream-Riken transcripts ciRS-7-null mice. If ciRS-7 transcription originates from a
322 promoter shared with C230004F18Rik, as is the case for human transcription, then ciRS-7
323 would originate from the same linear pre-spliced transcript as the Riken transcripts. This raises
324 the possibility that generating linear transcripts containing the ciRS-7 sequence destabilizes
325 them or that the act of circRNA biogenesis itself leads to destabilization of the residual linear
326 transcript. These explanations would predict upregulation of the Riken transcripts when the

327 ciRS-7 exon is deleted. Another model is that ciRS-7 could directly or indirectly affect
328 expression of the Riken transcripts through regulatory networks. For example, ciRS-7 may
329 sequester or compete for splicing factors (e.g., nuclear Ago2 [23]), or ciRS-7 expression may
330 affect the expression of other genes that are involved in direct regulation of the Riken
331 transcripts.

332 The view that ciRS-7 directly regulates its host transcript is supported by our finding that
333 ASINC transcripts are differentially localized in the cell depending on their inclusion of the ciRS-
334 7 sequence. This suggests active regulation of or by the transcripts potentially through factors
335 that bind the sequence in ciRS-7, and generates the hypothesis that ciRS-7-containing linear
336 ASINC.2 has different functions in the nucleus than the ciRS-7 circRNA in the cytoplasm.
337 Indeed, the cytoplasmic ciRS-7 circles have been shown to function by sequestering mir-7[6,7],
338 a mechanism that unlikely to be employed by nuclear ASINC.2. Further study of transcripts in
339 the entirety of the locus and their regulation may reveal new functions for ciRS-7 and this locus
340 as a whole.

341 This work also lays a foundation for the field to begin to dissect transcriptional regulation
342 and biogenesis of the ciRS-7 locus. Regulation of alternative splice variants in the ASINC locus,
343 transcription factor binding patterns, and three-dimensional interactions between the promoters
344 and putative enhancers we identified can now be analyzed across different cell types and
345 throughout development. In addition, the analysis presented here could be generalized to other
346 genes whose promoters are not well-annotated. For example, another well-known circRNA with
347 no annotated promoter is derived from the Sry gene in mouse, which is circularized in mature
348 adult testes but expresses an unspliced mRNA in the developing genital ridge that governs sex
349 determination [2]. It has been hypothesized, though remains untested, that the promoter for the
350 Sry circRNA uses a separate promoter from the linear mRNA[24]. Other highly-expressed
351 circRNAs in human are also derived from the first exon of an annotated mRNA [25]. Given our
352 results, we predict that the promoters of these circular RNAs may have been misidentified

353 and/or misannotated in the genome and may be associated with cryptic up- or downstream
354 splice junctions. Future analyses that comprehensively characterize transcription and splicing
355 at individual loci will be required to fully understand the regulatory mechanisms underlying
356 circRNA biogenesis.
357

358 ## Methods

359

360 **RNA-seq analysis for detection of novel splice isoforms**

361 Raw RNA-seq reads from SRR5048080 (human) and SRR1785046 (mouse) were downloaded
362 from the SRA. Reads were mapped and analyzed using KNIFE [27]. Reads failing to align
363 ("unaligned") by KNIFE were used in a simple custom mapping approach to identify novel
364 splicing events within a single read: single reads were split into pseudo-pairs (k-mers) by taking
365 the first 20 mer in the unaligned read and the remaining k-mer defined by the start position O
366 (30 for mouse and 50 for human because of differing input read lengths) and the minimum of
367 O+20 and the remaining read length after trimming (see supplemental perl script in S2 File).
368 Only reads where each pseudo-pair > 18 nt were used for analysis. These pseudo-paired end
369 reads, which actually came from the same single read were then realigned separately as pairs
370 using bowtie2 to a custom index made by the following sequences:
371

372 >mm10_knownGene_uc012hid.1 range=chrX:61083246-61285558 5'pad=0 3'pad=0 strand=-
373 repeatMasking=none
374 >hg38_knownGene_uc004fbf.2 range=chrX:140683176-140884660 5'pad=0 3'pad=0 strand=+
375 repeatMasking=none
376

377 Pairs of pseudo-reads mapping on the same strand were identified and used for further
378 analysis. While pseudo-alignments are used in some RNA-seq analysis approaches, few
379 algorithms are capable of achieving precise de novo transcript recovery due to their high false
380 positive rates and unknown false negative rates. This approach differs from other algorithms
381 because it (a) does not use a seed and extend approach; and (b) reads are aligned to a 100 kb
382 radius of ciRS-7 rather than the reference genome, in principle, preventing misalignment of true
383 ASINC reads to other loci. The complete analysis, the R script used along with output is
384 provided in S2 File. Although our analysis is likely to include other novel splicing in the locus, we
385 focused our attention on queries for reads that supported a splice from an un-annotated location
386 upstream of the acceptor in ciRS-7 and from the donor in ciRS-7 to an un-annotated
387 downstream exon using criteria on the position of discordant pseudo-paired end mappings (see
388 R script). An example of the reads that supported these events were (in human:
389 SRR5048129.92905492_2774860 (upstream exon); SRR5048080.59411858_2626289
390 (downstream exon) and in mouse: SRR1785046.9826290 (upstream exon);
391 @SRR1785046.13497132 HWI-ST1148:158:C3UJCACXX:2:2112:5228:93046 length=50
392 (downstream exon backsplicing to ciRS-7 acceptor).
393
394
395 **ENCODE data analysis**
396 For ChIP-seq analysis of histone modifications, processed narrowPeak files aligned to hg19
397 were downloaded from the ENCODE portal. All samples for ChIP-seq were selected with the
398 following filtering criteria, based on annotations in the metadata annotation file downloaded from
399 https://www.encodeproject.org/metadata/type=Experiment&replicates.library.biosample.donor.or
400 ganism.scientific_name=Homo+sapiens/metadata.tsv: “Assay” == “ChIP-seq”, “File format” ==
401 “bed narrowPeak”, “Output type” == “peaks”. Only samples with availability of H3K4me1,
402 H3K4me3, H3K9me3, H3K27ac, H3K27me3, and H3K36me3 were selected. For RNA-seq

403 analysis, raw reads were similarly downloaded from the ENCODE portal. Total RNA-seq
404 experimental data were filtered based on the following criteria: “File format” == “fastq”, “Output
405 type” == “reads”, “Biosample treatment” == null, “Library depleted in” == “rRNA”, “Biosample
406 subcellular fraction term name” == null. The lists of cell types for which satisfactory ChIP-seq
407 and RNA-seq data were cross-referenced to identify the list of 34 cell types for which data was
408 analyzed.
409
410 ChIP-seq narrowPeak file were processed according to the following pipeline: the enrichment
411 scores of any peak calls in genomic 500bp bins spanning 50 kb up- and down-stream of the
412 genomic locus were identified using bedtools intersect -wao -a [genomic_bins.bed] -b
413 [narrowPeak file]. If multiple peaks were called in a given bin, the peak with the highest
414 enrichment score was reported using bedtools merge -c [enrichment column] -o max. The
415 absence of a peak was reported as a 0, which could indicate either complete lack of signal or
416 insufficient signal over input to call a significant peak in the ENCODE pipeline. Fold enrichment
417 values for replicate ChIP-seq experiments performed on the same cell type were averaged for a
418 given genomic bin.
419
420 RNA-seq reads were quantified using kallisto quant against a custom kallisto index consisting of
421 RefSeq cDNA transcripts, exclusive of any covering the ASINC/CiRS-7 locus, plus sequences
422 corresponding to individual ASINC/ciRS-7 exons transcribed from both the plus and minus
423 strands[28]. For single-ended data, the quant --[fr/rf]-stranded -b 0 -t 2 -l 200 -s 20 --single
424 command was used, using either --fr-stranded or --rf-stranded depending on the order of the
425 input files. For paired-ended data, the quant --[fr/rf]-stranded -b 0 -t 2 command was used, again
426 using either --fr-stranded or --rf-stranded depending on the input read files.
427 Expression data was quantified as 1000*tpm/transcript length. Expression values (RPKM) were
428 averaged across replicates for a given cell type for a given transcript.

429

430 Our methodology for identifying novel promoters is described below and fundamentally differs
431 from typical informatic approaches such as machine-learning algorithms that use hidden
432 variables or neural networks. These approaches have unknown statistical properties such as
433 effective degrees of freedom or an easily-modeled null distribution for the final test statistic.
434 Below, we describe a method that is conceptually simple and statistically transparent in that the
435 null distribution can be easily computed, and our statistic of interest, numerically related to the
436 active promoter, can be referred to this distribution to obtain an empirical p value.
437 Decoy ChIP marks on chromosomes 7, 12, and X, corresponding to regions +/- 50 kb upstream
438 and downstream of the annotated TSS and transcription stop sites respectively in the ACTB,
439 FOXO4, and HOTAIR loci, were used as an empirical null for determining the false-discovery
440 rate (FDR) for correlations between ChIP enrichment in putative promoters and enhancers (S3
441 File). We computed an FDR as follows. For each mark, we computed the correlation between
442 ciRS-7, measured as exonic TPM, and chromatin mark enrichment for bins on chromosomes 7,
443 12, and X, and generated the empirical distribution of these correlations (S5 File). Then for each
444 mark, we determined the correlation value above which 0.5% of the data in the empirical null fell
445 ($q<0.005$), and assigned a correlational threshold on the basis of this. We model-checked our
446 assumptions for the empirical null distribution by showing that there was no significant
447 correlation or anticorrelation between ciRS-7 and ACTB (Pearson $r = 0.31$, p-value = 0.08),
448 ciRS-7 and HOTAIR (Pearson $r = -0.13$, p-value = 0.45), or ciRS-7 and FOXO4 (Pearson
449 $r=0.12$, p-value 0.48) as such effects could distort our null model. Heatmaps were generated by
450 averaging ChIP-seq peak enrichment for a given 500bp genomic bin across all sample
451 replicates, and computing the Pearson correlation coefficient of ChIP enrichment against RNA-
452 seq expression for a given cell type.

453 For genome browser screenshots, pre-processed data was obtained from the ENCODE portal
454 (see S6 File) and visualized using the UCSC genome browser. Data were shown as the mean
455 value over a smoothing window of 6 pixels.
456
457 **Quantification of novel junctions and isoforms from ENCODE RNA-seq data sets**
458 370 paired-end RNA-sequencing data sets made from ribosomal RNA-depleted total RNA were
459 downloaded from the ENCODE portal. This set included some samples for which there were
460 biological or technical replicates, representing 136 different cell/tissue types. FASTQ files were
461 quantified against a kallisto index made from ENSEMBL release 89 ncRNA and cDNA fasta files
462 using default parameters (kallisto index -k 31). A second custom kallisto index was created
463 from 40bp junctional sequences within the ASINC locus containing 20bp sequence upstream of
464 a splice site and 20bp sequence downstream of a splice site. This index was also created using
465 default parameters. Paired end data was downloaded and processed using kallisto quant -b 0
466 against both indexes. tpm (transcripts per million) outputs from the reference transcriptome
467 were aggregated, and for samples with multiple sequencing data sets, tpms were averaged
468 across replicates. For gene-level analysis of the ASINC locus, the five transcripts
469 corresponding to 'LINC00632' in ENSEMBL release 89 were summed to determine gene-level
470 expression of the locus. For the custom junctional index, est_counts output for each sample
471 from kallisto quant were normalized to sequencing depth calculated from the reference
472 transcriptome and averaged across replicates. Only junctions with reads supported by at least
473 one sample were reported.
474
475 **Analysis of mouse ciRS-7 knock-out data**
476 Data from Piwecka et al. [10] were downloaded from the NCBI Sequence Read Archive using
477 the tool fastq-dump. Data were quantified using kallisto quant --single -l 200 -s 30 against a
478 kallisto index built using default parameters. The kallisto index was generated from a

479 concatenation of cDNA and ncRNA from ENSEMBL release 90 with the addition of the
480 C030023E24Rik sequence, which was not present in the ENSEMBL fasta file. Kallisto
481 quantification was imported into R using tximport [29] and differential gene expression analysis was
482 performed using DESeq2 with default parameters [30]. Aggregation of transcript annotations to
483 perform gene-level analysis was performed with the tx2gene parameter of tximport based on
484 transcript-gene pairing information parsed from the ENSEMBL fasta files. Unless otherwise noted,
485 cutoffs for significance were based genes having an adjusted p-value ("padj") lower than 0.05.
486

487 **Bacterial Artificial Chromosomes (BACs) and plasmid vectors**

488 BACs were purchased from Thermo Fisher Scientific (Waltham, MA) in the case of BAC CTD-
489 2166E9, and from the BACPAC Resources Center (Children's Hospital Oakland Research
490 Institute, CA) in the case of all other BACs. BACs were purified from E. coli using the
491 Nucleobond Xtra BAC Maxi Kit (Macherey-Nagel, Duren, Germany). SP-dCAS9-VPR (Addgene
492 ID: 63798) was provided by the Qi lab[19], and the sgRNA-encoding plasmid along with the
493 Cas9 plasmid, pMCB306 (Addgene ID: 89360) and lentiCas9-Blast (Addgene ID: 52962)
494 respectively, were gifts from Michael Bassik [31,32]. Guides were cloned into pMCB306 cloned
495 into the BlpI/BstXI site using annealed oligos with the appropriate sticky ends (S1 File).
496

497 **BAC Fingerprinting**

498 To ensure BACs had the proper insert, 3 µg of each BAC were digested with 12 units of Ban I
499 (NEB, Ipswich, MA) in the manufacturer's buffer for 1.5 hours at 37°C. The digests were then
500 heated to 65°C for 20 min. The digestion fragments were separated by loading 750 ng per lane
501 on a 1% LE Agarose (GeneMate) gel with 0.5X TAE running buffer. The DNA was visualized
502 with ethidium bromide staining. Simulated BAC fingerprints were created using SnapGene
503 software (from GSL Biotech) (S16 Fig).
504

505 **Transfections**

506 All transfections were performed in 6-well plates using 7.5 µL of Lipofectamine 3000 and 2.5 µg
507 of total DNA per well according to the manufacturer's protocol. Unless noted otherwise, cells
508 were harvested 24 hours after transfection.

509 For CRISPRa experiments, we introduced 1.25 µg of the SP-dCAS9-VPR plasmid and 1.25 µg
510 of combined sgRNA plasmids (four for each promoter tested) (see S1 File for sequences). Cells
511 were harvested 48 hours after transfection.

512 For CRISPR genomic deletions, two sgRNA vectors (pMCB306) with guides targeting a ~55 kb
513 deletion of the X chromosome were transfected into HEK293T cells at a total mass of 1.25 mg
514 per transfection along with 1.25 mg of a vector expressing Cas9 (lentiCas9-Blast). The
515 sequences for these guides can be found in S1 file. The cells were incubated for two days prior
516 to being sorted into single cells by GFP fluorescence as a measure of transfection, which is also
517 expressed on pMCB306. After two weeks, colonies were screened by PCR for the presence of
518 the deletion.

519

520 **Nuclear/Cytoplasmic Fractionation**

521 1-2x$10^6$ 293T cells were fractionated for nuclear/cytoplasmic RNA using the PARIS kit (Thermo
522 Fisher Scientific) according to the manufacturer's instructions. 0.25-0.5 µg of RNA of each
523 fractionated sample was used in the RT prior to qPCR, using an equal RNA mass for both the
524 nuclear and cytoplasmic fractions in each experiment.

525

526 **RNA Purification (primary tissue)**

527 Snap-frozen total brain tissue from a 12-week old C57BL/6 pregnant female mouse was
528 homogenized in TRIZOL and the aqueous phase was purified on Purelink RNA column with on-
529 column DNase treatment.

530

531 **RNA Purification (cell lines)**

532 Cells were lysed directly in tissue culture plates by the direct addition of TRIzol reagent (Thermo
533 Fisher Scientific). The manufacturer's protocol was followed with the following modifications:
534 after isolation of the aqueous phase, 1 volume of 100% EtOH was added to the sample, and
535 then the entire volume was applied to and spun through a RNA Clean & Concentrator-5 column
536 (Zymo, Irvine, CA). The column protocol was performed as per the manual's instructions starting
537 from the application of the RNA Prep Buffer.

538

539 **RNase R treatment**

540 1 µg of RNA was treated with 5 U RNase R (Epicentre, Madison, WI) (or no enzyme in the case
541 of the mock) in 10 µL total reaction volume at 37 C for 30 min. 1 µL 1 mM EDTA, 10 mM
542 dNTPs, and 25 uM random hexamers were then added to the sample and the sample was then
543 heated to 65 C for 5 min to denature RNA structures. The RNA was then reverse transcribed
544 without purification with the addition of 4 µL 5x supplement buffer (250 mM Tris pH 8, 125 mM
545 KCl, 15 mM MgCl2) and 2 µL of 0.1 M DTT to provide the necessary conditions for the RT
546 reaction.

547

548 **RT-PCR and qPCR**

549 Total RNA was reverse transcribed with random hexamers using 100 U Maxima Reverse
550 Transcriptase (Thermo Fisher Scientific) according to the manufacturer's instructions.
551 Endpoint PCRs were performed using DreamTaq DNA Polymerase (Thermo Fisher Scientific,
552 Waltham, MA). For all PCR reactions, 1.5 µl of the unpurified RT-reaction was used per 50 µl
553 reaction volume. All RT-PCR reactions were performed using the recommended cycling
554 protocol for 35 cycles.
555 qPCR reactions were assembled as 10 µl reactions using AccuPower 2X GreenStar qPCR
556 Master Mix (Bioneer, Daejeon, Korea) with 0.3 µl of template used per reaction. qPCRs were

557 performed on an ABI 7900HT using following cycling protocol: 50℃ for 20 min, 95℃ for 10 min,
558 (95℃ for 15 s and 60˚C for 60 s) × 45 cycles, followed by a dissociation stage.
559
560 **Northern Blot**
561 Northern Blots were performed using 5 μg of total RNA per well using the NorthernMax kit
562 (Thermo Fisher Scientific) according to the manufacturer's recommendations. Single-stranded
563 DNA oligos were used as probes and were purchased from IDT (Coralville, IA). Probe
564 sequences can be found in S1 File.
565

## 566 Supporting Information

567 **S1 Fig. Additional ChIP-seq plots across the ciRS-7 locus from neuronal and HeLa cells.**
568
569 **S2 Fig. Heatmap of pearson correlations between chip marks at null loci and ciRS-7**
570 **expression**: ACTB (top), HOTAIR (middle), FOXO4 (bottom). Coordinates reported are from the
571 hg19 genome build.
572
573 **S3 Fig. Sample correlational plots of chip mark enrichment vs ciRS-7 expression at the distal**
574 **promoter region.**
575
576 **S4 Fig. CRISPR activation of LINC00632 promoters induces the expression of ciRS-7 in HeLa**
577 **cells.** qPCR measurement of ciRS-7 expression relative to actin. Error bars represent the
578 standard deviation of biological replicates.
579
580 **S5 Fig. RNase R sensitivity of transcripts generated from BAC O vs HEK293T.** LINC00632

581 isoform T3 was measured in both cases. Error bars represent the standard deviation of
582 biological replicates.
583
584 **S6 Fig.Transfection efficiency of the BACs** relative to BAC O quantified by DNA-qPCR of
585 BAC backbone DNA from HeLa cells transfected with the BAC. Error bars represent the
586 standard deviation of biological replicates (with error propagated from BAC O).
587
588 **S7 Fig. qPCR quantification of ciRS-7 and LINC00632 isoform T3 in HeLa transfected with**
589 **BACs and HEK mutants.** (A) RNA expression in HeLa transfected with BACs A, B, and C. All
590 values have been normalized to those for BAC A, and error bars represent the standard
591 deviation of biological replicates (with error propagated from BAC A). (B) RNA expression of
592 isoforms in wild-type HEK293T and in a cloned strain of HEK293T in which the putative ciRS-7
593 promoters have been deleted.
594
595 **S8 Fig. Additional PCRs to determine connectivity between exons of LINC00632 and ciRS-**
596 **7.**
597
598 **S9 Fig. Sanger sequencing traces for novel linear ciRS-7 junctions in human.**
599
600 **S10 Fig. Products from TOPO cloning** of bands in Fig 2B--*left* (lanes 2 and 3).
601
602 **S11 Fig. qPCR ΔCt of human isoforms.** Higher values indicate lower expression. Error bars
603 represent standard deviation of biological replicates.
604

605 **S12 Fig. RNase R sensitivity of ciRS-7, LINC00632, and LINC00632-CDR1AS isoforms in**
606 **HEK293T.**
607
608 **S13 Fig. Quantification of ciRS-7 and LINC00632 transcripts across ENCODE tissues and cell**
609 **lines.** (A) LINC00632 and ciRS-7 gene-level quantification, transcripts per million reads (tpm) (B)
610 ciRS-7 backsplice and LINC00632-ciRS-7 junctional counts per million reads
611
612 **S14 Fig. qPCR ΔCt of mouse isoforms** *(Top)* ΔCt (vs GAPDH) for ciRS-7 linear and circular
613 isoforms and (*Bottom*) RNase R sensitivity of transcripts in mouse brain. Error bars represent
614 standard deviation of technical replicates.
615
616 **S15 Fig. Volcano plots of log fold-change ciRS-7 KO vs WT in each brain region (Methods).**
617
618 **S16 Fig. BAC quality checks.** (A) Simulated and experimental BanI digest of the four BACs
619 used in this study. The agreement of these footprints supports that BAC inserts are as reported
620 and have not been significantly altered by bacterial recombination. (B) Sanger sequencing of
621 the 5' ends of BAC genomic inserts. The vector sequence is in lowercase; the genomic insert
622 sequence is in uppercase.
623
624 **S1 File. PCR primers, Northern probes, and sgRNA sequences.**
625 **S2 File. RNA-seq scripts and output for novel isoform discovery.**
626 **S3 File. Table of ChIP-seq peak enrichment and RNA expression levels.**
627 **S4 File. Quantification of RNA expression in ENCODE data.**
628 **S5 File. Calculation of empirical FDR for ChIP-seq and RNA-seq correlations.**

**S6 File. ENCODE accession numbers used in genome browser screenshots.**

## Acknowledgments

We thank Peter Wang, Peter Sarnow, Zoe Davis and Robert Bierman for discussion and critical comments that improved our work; Roozbeh Dehghannasiri for help with analysis, the Krasnow and Herschlag Labs for discussions, sharing reagents and space; the Qi and Bassik labs for plasmids, and Inga Jarmoskaite for her help with radiation safety training.

## References

1. Salzman J, Gawad C, Wang PL, Lacayo N, Brown PO (2012) Circular RNAs are the predominant transcript isoform from hundreds of human genes in diverse cell types. PLoS ONE 7: e30733. doi:10.1371/journal.pone.0030733.

2. Capel B, Swain A, Nicolis S, Hacker A, Walter M, et al. (1993) Circular transcripts of the testis-determining gene Sry in adult mouse testis. Cell 73: 1019–1030. doi:10.1016/0092-8674(93)90279-Y.

3. Jeck WR, Sorrentino JA, Wang K, Slevin MK, Burd CE, et al. (2013) Circular RNAs are abundant, conserved, and associated with ALU repeats. RNA 19: 141–157. doi:10.1261/rna.035667.112.

4. Nigro JM, Cho KR, Fearon ER, Kern SE, Ruppert JM, et al. (1991) Scrambled exons. Cell 64: 607–613. doi:10.1016/0092-8674(91)90244-S.

5. Wang PL, Bao Y, Yee M-C, Barrett SP, Hogan GJ, et al. (2014) Circular RNA is expressed across the eukaryotic tree of life. PLoS ONE 9: e90859. doi:10.1371/journal.pone.0090859.

6. Memczak S, Jens M, Elefsinioti A, Torti F, Krueger J, et al. (2013) Circular RNAs are a large class of animal RNAs with regulatory potency. Nature 495: 333–338. doi:10.1038/nature11928.

7. Hansen TB, Jensen TI, Clausen BH, Bramsen JB, Finsen B, et al. (2013) Natural RNA circles function as efficient microRNA sponges. Nature 495: 384–388. doi:10.1038/nature11993.

8. Hansen TB, Wiklund ED, Bramsen JB, Villadsen SB, Statham AL, et al. (2011) miRNA-dependent gene silencing involving Ago2-mediated cleavage of a circular antisense RNA. EMBO J 30: 4414–4422. doi:10.1038/emboj.2011.359.

9. Rybak-Wolf A, Stottmeister C, Glažar P, Jens M, Pino N, et al. (2015) Circular rnas in the mammalian brain are highly abundant, conserved, and dynamically expressed. Mol Cell 58: 870–885. doi:10.1016/j.molcel.2015.03.027.

663 10. Piwecka M, Glažar P, Hernandez-Miranda LR, Memczak S, Wolf SA, et al.
664 (2017) Loss of a mammalian circular RNA locus causes miRNA deregulation and affects
665 brain function. Science 357. doi:10.1126/science.aam8526.

666 11. Liang D, Wilusz JE (2014) Short intronic repeat sequences facilitate circular RNA
667 production. Genes Dev 28: 2233–2247. doi:10.1101/gad.251926.114.

668 12. Kramer MC, Liang D, Tatomer DC, Gold B, March ZM, et al. (2015)
669 Combinatorial control of Drosophila circular RNA expression by intronic repeats, hnRNPs,
670 and SR proteins. Genes Dev 29: 2168–2182. doi:10.1101/gad.270421.115.

671 13. Ivanov A, Memczak S, Wyler E, Torti F, Porath HT, et al. (2015) Analysis of
672 intron sequences reveals hallmarks of circular RNA biogenesis in animals. Cell Rep 10:
673 170–177. doi:10.1016/j.celrep.2014.12.019.

674 14. Liang G, Lin JCY, Wei V, Yoo C, Cheng JC, et al. (2004) Distinct localization of
675 histone H3 acetylation and H3-K4 methylation to the transcription start sites in the human
676 genome. Proc Natl Acad Sci U S A 101: 7357–7362. doi:10.1073/pnas.0401866101.

677 15. Wang Z, Zang C, Rosenfeld JA, Schones DE, Barski A, et al. (2008)
678 Combinatorial patterns of histone acetylations and methylations in the human genome.
679 Nat Genet 40: 897–903. doi:10.1038/ng.154.

680 16. Barski A, Cuddapah S, Cui K, Roh T-Y, Schones DE, et al. (2007) High-
681 resolution profiling of histone methylations in the human genome. Cell 129: 823–837.
682 doi:10.1016/j.cell.2007.05.009.

683 17. Zhang Y, Liu T, Meyer CA, Eeckhoute J, Johnson DS, et al. (2008) Model-based
684 analysis of ChIP-Seq (MACS). Genome Biol 9: R137. doi:10.1186/gb-2008-9-9-r137.

685 18. Creyghton MP, Cheng AW, Welstead GG, Kooistra T, Carey BW, et al. (2010)
686 Histone H3K27ac separates active from poised enhancers and predicts developmental
687 state. Proc Natl Acad Sci U S A 107: 21931–21936. doi:10.1073/pnas.1016071107.

688 19. Chavez A, Scheiman J, Vora S, Pruitt BW, Tuttle M, et al. (2015) Highly efficient
689 Cas9-mediated transcriptional programming. Nat Methods 12: 326–328.
690 doi:10.1038/nmeth.3312.

691 20. Engström PG, Steijger T, Sipos B, Grant GR, Kahles A, et al. (2013) Systematic
692 evaluation of spliced alignment programs for RNA-seq data. Nat Methods 10: 1185–1191.
693 doi:10.1038/nmeth.2722.

694 21. Lasda E, Parker R (2016) Circular RNAs Co-Precipitate with Extracellular
695 Vesicles: A Possible Mechanism for circRNA Clearance. PLoS ONE 11: e0148407.
696 doi:10.1371/journal.pone.0148407.

697 22. Johnsson P, Lipovich L, Grandér D, Morris KV (2014) Evolutionary conservation
698 of long non-coding RNAs; sequence, structure, function. Biochim Biophys Acta 1840:
699 1063–1071. doi:10.1016/j.bbagen.2013.10.035.

700 23. Taliaferro JM, Aspden JL, Bradley T, Marwha D, Blanchette M, et al. (2013) Two
701 new and distinct roles for Drosophila Argonaute-2 in the nucleus: alternative pre-mRNA

splicing and transcriptional repression. Genes Dev 27: 378–389. doi:10.1101/gad.210708.112.

24. Hacker A, Capel B, Goodfellow P, Lovell-Badge R (1995) Expression of Sry, the mouse sex determining gene. Development 121: 1603–1614.

25. Zhang X-O, Wang H-B, Zhang Y, Lu X, Chen L-L, et al. (2014) Complementary sequence-mediated exon circularization. Cell 159: 134–147. doi:10.1016/j.cell.2014.09.001.

26. Farh KK-H, Grimson A, Jan C, Lewis BP, Johnston WK, et al. (2005) The widespread impact of mammalian MicroRNAs on mRNA repression and evolution. Science 310: 1817–1821. doi:10.1126/science.1121158.

27. Szabo L, Morey R, Palpant NJ, Wang PL, Afari N, et al. (2015) Statistically based splicing detection reveals neural enrichment and tissue-specific induction of circular RNA during human fetal development. Genome Biol 16: 126. doi:10.1186/s13059-015-0690-5.

28. Bray NL, Pimentel H, Melsted P, Pachter L (2016) Near-optimal probabilistic RNA-seq quantification. Nat Biotechnol 34: 525–527. doi:10.1038/nbt.3519.

29. Soneson C, Love MI, Robinson MD (2015) Differential analyses for RNA-seq: transcript-level estimates improve gene-level inferences. [version 2; referees: 2 approved]. F1000Res 4: 1521. doi:10.12688/f1000research.7563.2.

30. Love MI, Huber W, Anders S (2014) Moderated estimation of fold change and dispersion for RNA-seq data with DESeq2. Genome Biol 15: 550. doi:10.1186/s13059-014-0550-8.

31. Han K, Jeng EE, Hess GT, Morgens DW, Li A, et al. (2017) Synergistic drug combinations for cancer identified in a CRISPR screen for pairwise genetic interactions. Nat Biotechnol 35: 463–474. doi:10.1038/nbt.3834.

32. Sanjana NE, Shalem O, Zhang F (2014) Improved vectors and genome-wide libraries for CRISPR screening. Nat Methods 11: 783–784. doi:10.1038/nmeth.3047.

# Figures

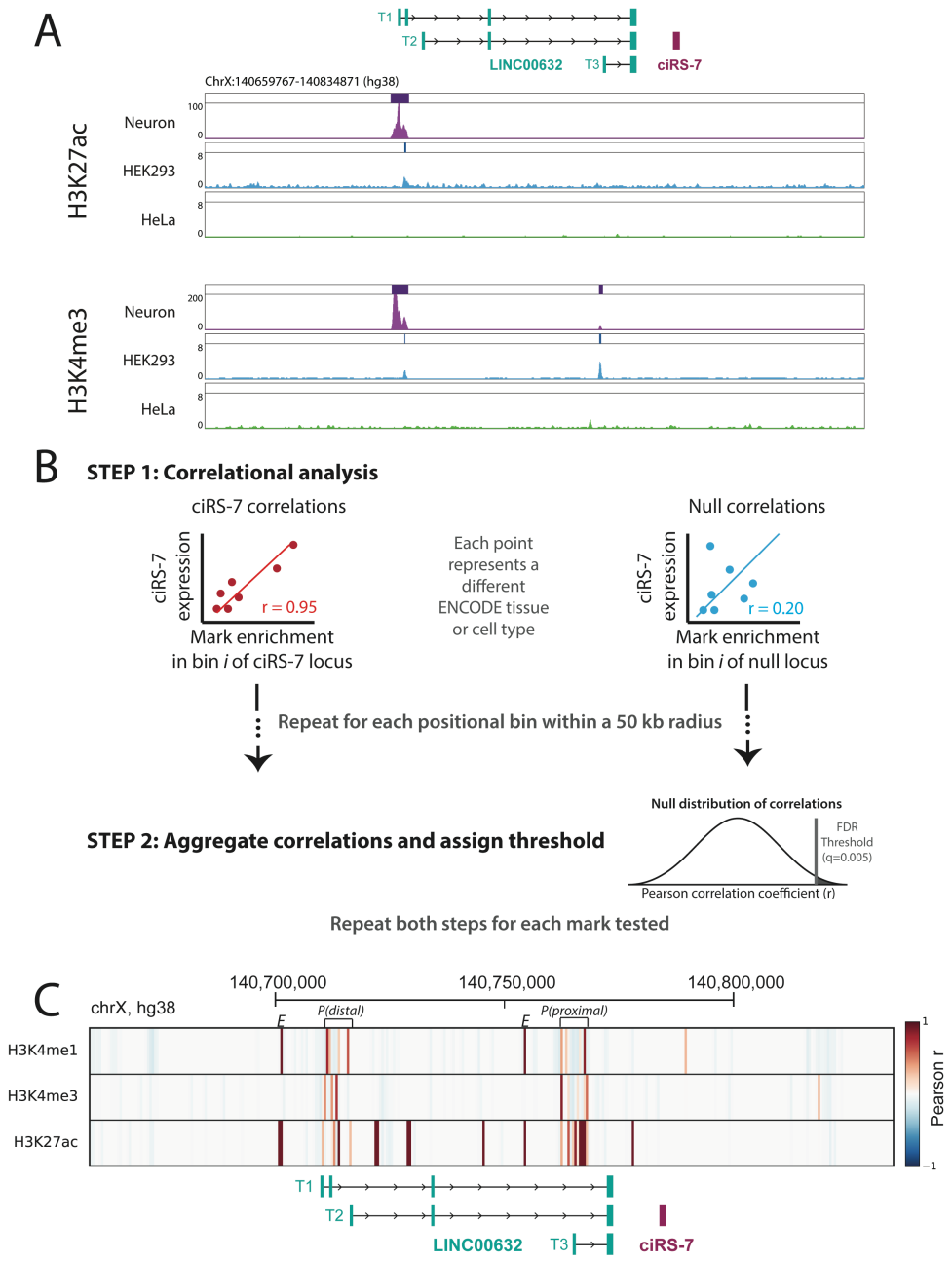


***Fig 1.*** Computational and statistical analysis predict ciRS-7 shares a promoter with annotated LINC isoforms. **(A)** H3K27ac and H3K4me3 peaks across the ciRS-7 locus and nearby genomic region in *in vitro*-differentiated neurons, HEK293, and HeLa cells. **(B)** Schematic depicting analysis correlating chromatin mark enrichment near the ciRS-7 locus with ciRS-7 expression in RNA seq data. To estimate a false discovery rate, null correlations are computed using chIP-enrichment at disparate regions of the genome with no relationship to ciRS-7 (ACTB, FOXO4, and HOTAIR). Then, using these null correlations, a null distribution is created from which a false discovery rate can be estimated. **(C)** Heatmap correlation (Pearson r) between strand-

specific ciRS-7 expression and enrichment of histone marks across the ciRS-7 locus and surrounding genomic region (spanning from 50 kb upstream of LINC00632 and 50 kb downstream of ciRS-7). Correlations are plotted in 500 nucleotide bins, and a depiction of annotated genes is shown below. Our FDR threshold (q<0.005) is satisfied for correlations greater than 0.35 for H3K4me1 (top 6 correlated bins), 0.45 for H3K4me3 (top 4 correlated bins), and 0.75 for H3K27ac (top 14 correlated bins) (See File S5). Putative promoters regions are annotated with brackets and the letter 'P'. Putative enhancers are marked with the letter 'E'.

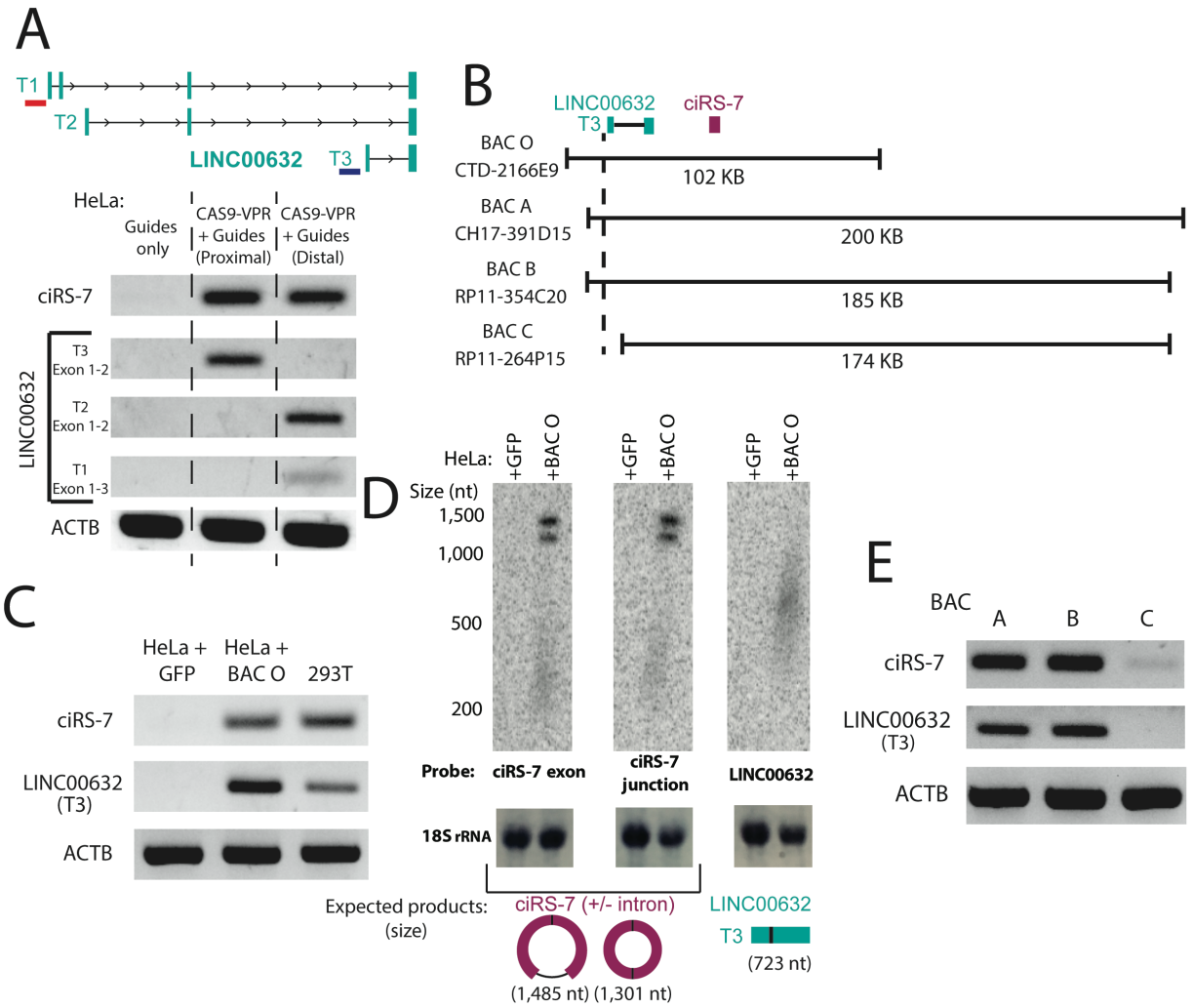


***Fig 2.*** Experimental approaches confirm the identity of the ciRS-7 promoter. **(A)** RT-PCR for ciRS-7 and LINC00632 transcripts in HeLa (+/- Cas9-VPR activation) with guide RNAs targeting distal and proximal promoters identified in Fig 1C. The approximate targeted locations of the proximal and distal guide RNAs are shown with a blue and red bar, respectively, in the diagram shown above the gel. **(B)** Schematic of BAC inserts with respect to the ciRS-7 and LINC00632 genes. **(C)** RT-PCR and **(D)** Northern blot for ciRS-7 and LINC00632 transcripts generated after BAC O transfection. The appearance of two bands in the ciRS-7 Northern blots are due to alternative splicing of an intron contained within the ciRS-7 exonic sequence. **(E)** RT-PCR for ciRS-7 and LINC00632 transcripts from HeLa cells transfected with BACs A-C.

763

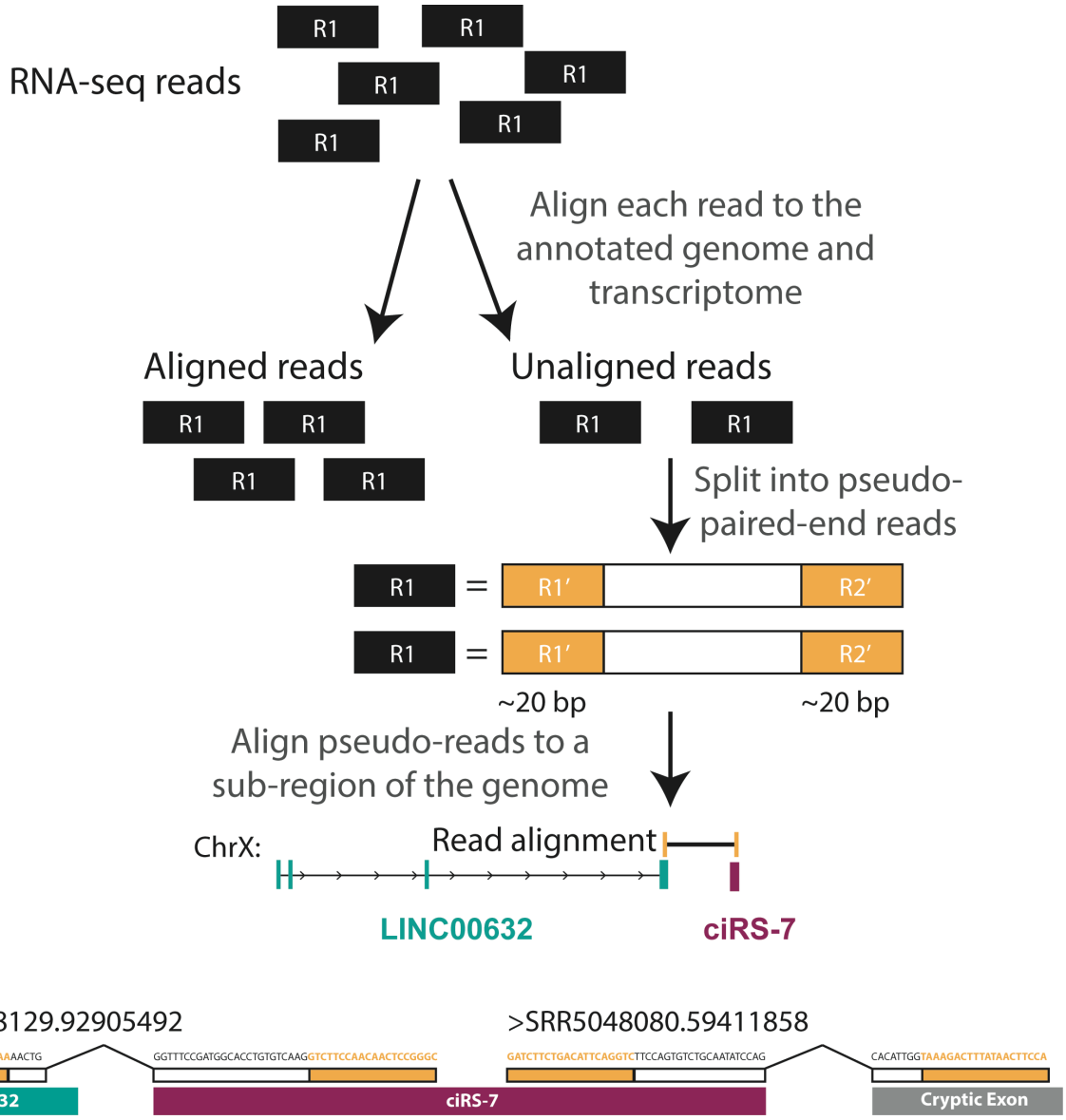


764

765 ***Fig 3.*** (Upper) Schematic outlining RNA-seq split read mapping approach. (Lower) Unannotated
766 linear splicing is predicted up- and downstream of the ciRS-7 exon. Reads supporting these
767 junctions are shown above the locus. Note, features are not drawn to scale.
768

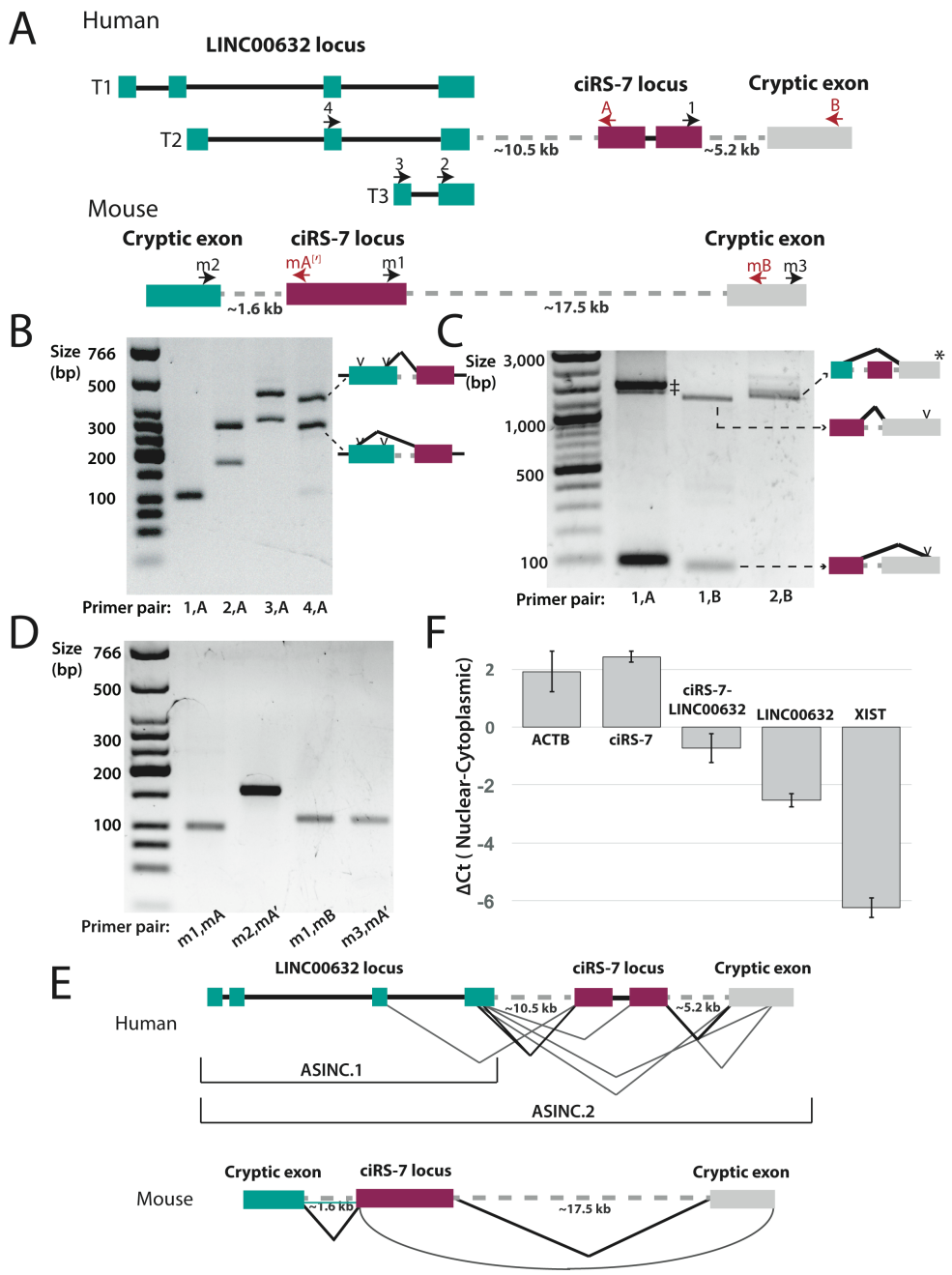


***Fig 4.*** ciRS-7 exonic sequence is included in linear transcripts. **(A)** Schematic of the locus including PCR primers used in this study. Dotted lines indicate approximate positions of newly discovered introns. Figure is not drawn to scale. **(B)** RT-PCR of circular and linear ciRS-7 splice products from HEK293T. (1,A): control PCR for ciRS-7; other lanes: LINC00632 exons spliced to the ciRS-7 exonic sequence: the two bands in each of these lanes represent the products formed when the two possible splice sites in the final exon of LINC00632 are used (see diagram on the right of gel). **(C)** PCR of spliced products that include cryptic exons downstream of ciRS-7. (‡) represents rolling circle ciRS-7 PCR products with and without intron retention. (*) Other products were also identified (see S7 Fig). **(D)** RT-PCR of circular and linear ciRS-7 splice products from mouse brain RNA. mA and mA' bind to approximately the same region but have slightly different sequence (see S1 File). **(E)** Examples of novel splicing observed in the human

781 and mouse ASINC loci. Curved line in mouse indicates a backsplice. **(F)** qPCR quantification of
782 nuclear-cytoplasmic fractionated RNA from HEK293T. Error bars represent the standard
783 deviation of biological replicates.

784

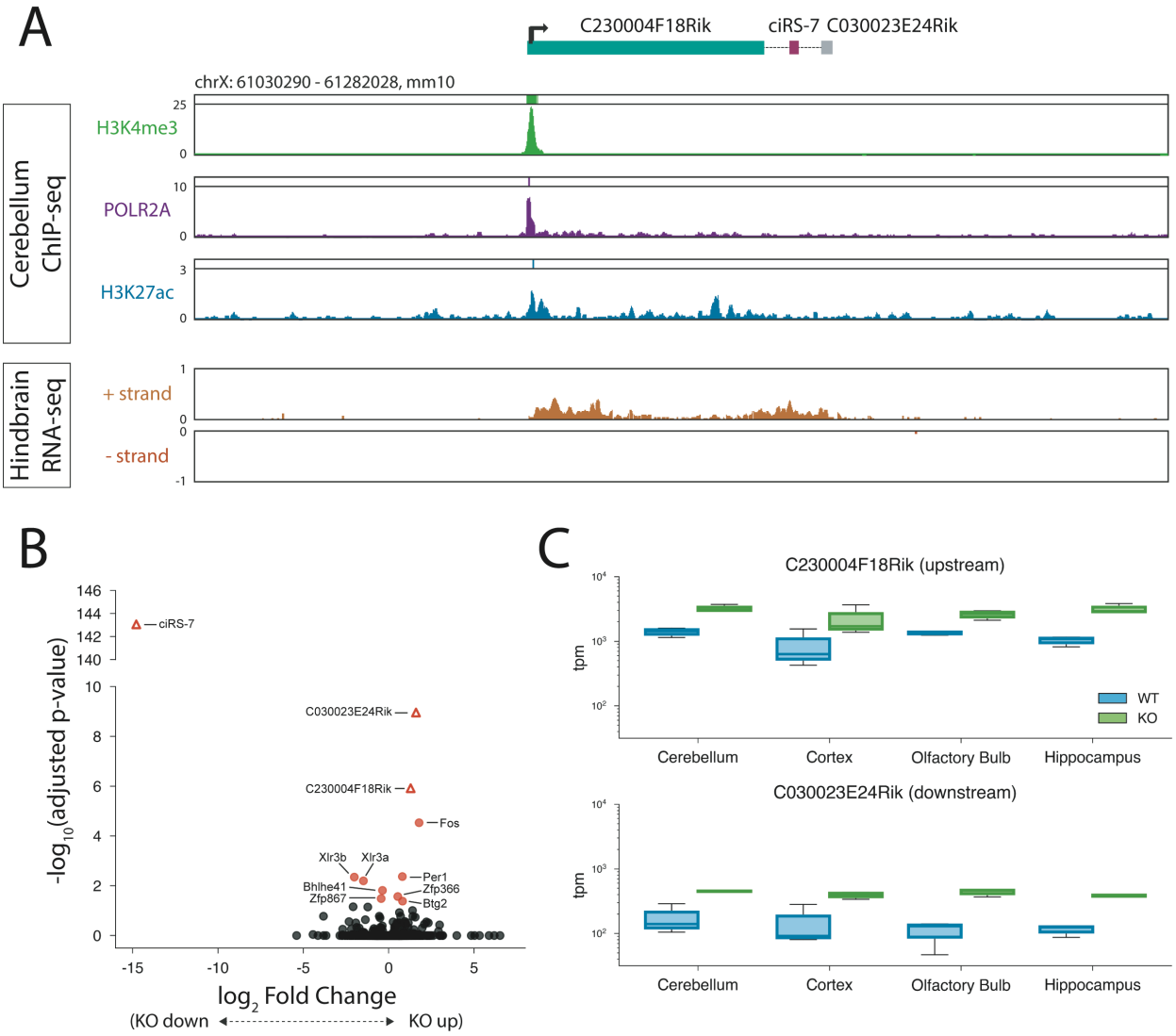


785

786 ***Fig 5.*** Up- and downstream transcripts are upregulated in ciRS-7 KO mouse. **(A)** ChIP-seq and
787 RNA-seq tracks for mouse cerebellum and hindbrain in the genomic region surrounding the
788 ciRS-7 locus. **(B)** Volcano plots of log fold-change ciRS-7 KO vs WT collapsed across four brain
789 regions. **(C)** Box plots depicting tpm of C230004F18Rik (top) and C030023E24Rik (bottom) in
790 WT and ciRS-7 KO mice across four brain regions.
791